Challenges in attributing the 2022 Australian rain bombs to climate change

Camille Cadiou, Robin Noyelle, Nemo Malhomme, Davide Faranda

Challenges in attributing the 2022 Australian rain bombs to climate change

Camille Cadiou[1†], Robin Noyelle[1†], Nemo Malhomme[1†] and Davide Faranda[1,2,3*]

[1]Laboratoire des Sciences du Climat et de l'Environnement, LSCE/IPSL, CEA-CNRS-UVSQ, Université Paris-Saclay, Gif-sur-Yvette, 91191, France.
[2]London Mathematical Laboratory, 8 Margravine Gardens London, W6 8RH, London, United Kingdom.
[3]LMD/IPSL, Ecole Normale Superieure, PSL research University, Paris, France.

*Corresponding author(s). E-mail(s): davide.faranda@cea.fr;
Contributing authors: camille.cadiou@lsce.ipsl.fr;
robin.noyelle@lsce.ipsl.fr; nemo.malhomme@lsce.ipsl.fr;
†These authors contributed equally to this work.

Abstract

In February and March 2022, the eastern coast of Australia recorded an unprecedented amount of precipitation with extended floods and damages to properties amounting at least to AUD 2.3 billions. In this paper we use both reanalysis and observations to perform a statistical and dynamical attribution of this precipitation event to climate change. We define 1948-1977 as the counterfactual period and 1990-2019 as the factual one. The statistical attribution is based on fitting the generalized extreme value distribution for 3-days averaged precipitation annual maxima for the two periods, while the dynamical attribution aims at looking at the recurrence properties of sea-level pressure and geopotential height patterns in both periods. We find that the dynamics of the event consists in an unprecedented combination of several factors: a tropical atmospheric river, the presence of the Coral low pressure system and a blocking anticyclone offshore Eastern Australia. Our main finding is that no clear attribution statements can be made, both because of the unprecedented nature of this

event, the lack of long high quality available data and the dependence of the results on the La Nina phase of El Nino Southern Oscillation.

Keywords: Climate Change, Extreme Precipitation, Attribution, Australia

1 Introduction

In the latest IPCC report (Masson-Delmotte et al, 2021), researchers confirm the role that human activity plays in the climate upheavals of recent decades. The scientists also confirm the role of anthropogenic greenhouse gases emissions in modifying frequency and intensity of extreme weather events that we experience today. The IPCC scientists warn in particular about the effects that climate change is having on the water cycle. Studies have shown that rising temperatures are leading to more intense rainfall, flooding but also to more severe droughts (Cook et al, 2018) in some regions of the world. The distribution, frequency and intensity of precipitations are changing significantly across the globe, especially in subtropical regions accustomed to monsoons (Douville et al, 2021). In the 21st century, coastal areas are already experiencing and will increasingly experience flooding due to heavy precipitations and sea level rise (Wilby and Keenan, 2012). Flooding from rising seas, which was only occasional a few decades ago, could occur every year by the end of the century (Hirabayashi et al, 2013).

Australian average land temperatures have risen by 1.44°C since 1910, according to the recent study by Grainger et al (2022). The oceans surrounding the continent have also warmed by an average of one degree over the same period, leading to more frequent marine heat waves. Half of the corals in Australia's Great Barrier Reef have died since 1995 because of this rise in water temperature in conjunction with increased acidification (Wolff et al, 2018; Holland et al, 2020). There is a wide consensus on the fact that sea levels will rise in future climates, affecting Australian coasts (Church et al, 2006; Woodruff et al, 2013; Church et al, 2017). As in other regions, this will likely increase the hazards linked to storm surges associated with tropical cyclones. Other authors have also pointed out that rainfall has decreased in southwestern Australia as well as in the fire-ravaged southeast, while increasing in the north, which has been hit by major floods and destructive cyclones in recent years (Dey et al, 2019; Abram et al, 2021).

If climate change projections for Australia are worrying, the country is already experiencing severe extreme weather events. Indeed, climate change has already taken its toll on Australia (Head et al, 2014; Abram et al, 2021; Canadell et al, 2021), which has been hit by fires, drought and intense cyclones. In 2019-2020 the country was already ravaged by wildfires of exceptional proportions after experiencing the hottest and driest year on record (Borchers Arriagada et al, 2020; Jetten et al, 2021). The fires destroyed an area almost the size of the United Kingdom, killed several people and killed

or displaced nearly three billion animals, costing the Australian economy about 7 billion AUD (Filkov et al, 2020). In the current 2022 year, both high and low temperature records have been broken in Australia. On one hand, on the 13/01, the coastal town of Onslow reached an unprecedented 50.7°C, the hottest temperature ever recorded in Australia for sixty-two years(The Guardian, 2022). On the other hand, on the 02/06, the temperature at the Thredbo Top weather station reached -6.9°C and historic snowfalls for this time of year (The New Daily, 2022). Future projections of climate-related disasters for the coastal areas as well as the vast island-continent report an increasing risk of extreme events capable of heavily damaging natural ecosystems and impact health and agriculture (Hobday et al, 2018; Dey et al, 2019; Ukkola et al, 2020).

Here we will focus on the record-breaking extreme precipitation event which occurred from the last week of February to mid-March 2022, in the eastern coast of Australia. Heavy precipitations - 345mm of rain were recorded at Brisbane on the 28th of February - met soils already close to saturation from the recent rains in the end of 2021. This lead to severe and enduring flooding in March. This event caused 22 recorded casualties, rendered uninhabitable 25,000 homes and businesses, forced 200,000 people to evacuate and produced massive power and transports outages for a total of ∼2.32 billion AUD of damage (Foreign Policy, 2022).

In order to explain this rain bomb event, we have identified two main ingredients: i) an atmospheric river, formed north the continent around the 22nd of February, in the upper atmosphere – between eight and 10 kilometres up – moved from the ocean to the south reaching the continent and producing a continuous flux of precipitation originating from the tropics, and ii) a dipolar structure consisting of a low pressure system in the Coral Sea and a blocking anticyclone further east. The combination of these elements allowed to transport moist air from the tropics to the Coral Sea, and then condense the moisture that has then fallen as rain thanks to the low pressure, while winds were pushing rain over Queensland's south east. Precipitation was further enhanced by orographic effects. At an even larger scale, the phenomena were embedded in a strong La Nina phase, which induces additional air moisture in the south west Pacific and wind circulation patterns that could have played a role in the intensity of the event.

Preliminary results of the University of Melbourne reported by national and international newspapers (see, e.g. The Guardian (2022)) showed that on the 26th and 27th of February, the two days with heaviest rain, 16 times the water held by Sydney harbour (500 bn liters) flowed in the atmospheric river above Queensland. Indeed, during those days rainfall of over 400 millimetres was recorded across the greater Brisbane area. This would add up on the 28th February to a total of 676.8 millimetres of rainfall, the largest three, and seven, day total ever recorded in Brisbane. Another record breaking amount of rainfall was recorded in Mount Glorious which received rainfall in excess of 1770 millimetres in the week until 28th of February. More than 30 locations across the south-east recorded rainfall in excess of 1000 millimetres, resulting in the

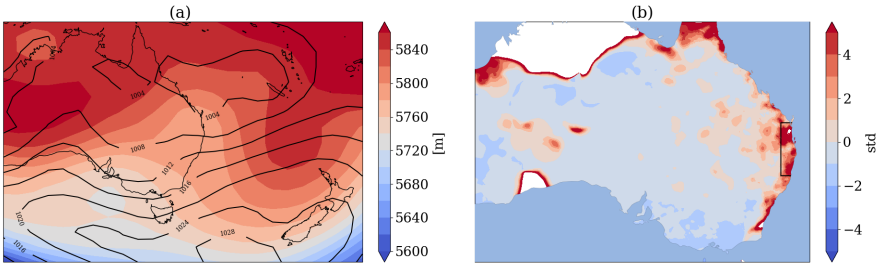

Fig. 1 Description of the rain bomb event. (a) Geopotential height at 500hPa (colors) and sea level pressure (contours) averaged over the 26th, 27th and 28th of February 2022. (b) Standardized anomaly of accumulated precipitations for the period 20th February - 20th March with respect to the 1990-2019 period. Regions in white correspond to standardized anomaly above 15 standard deviations.

floods being more intense than that of 1974. The unprecedented flooding that raised many rivers above record highs moved south, leaving towns underwater. The area of Sydney was more affected on the 3rd and the 8th of March with the city's chief reservoir, spilling at a rate in excess of 70 gigalitres a day on March 3. Residents in parts of western Sydney were told to evacuate for the second year in a row as the city's Warragamba Dam overflowed. But the system stalled before it passed over Sydney.

Damage from floods is only partially estimated at this stage, but is expected to reach almost AUD 2.3 billion (Foreign Policy, 2022), an estimate that exceeds that of the Insurance Council of Australia, which also summed-up the cost of claims from the disaster to AUD 1.45 billion (ClimateCouncilAustralia, 2022). However, this is only a lower bound, as the estimates are still expected to grow.

Figure 1 (a) presents the synoptic situation averaged over the 26th, 27th and 28th of February over the region. We see the dipole structure with an upper level low pressure system centered above the Brisbane region and a high pressure system over the Coral sea. Figure 1 (b) presents the standardized anomaly of accumulated precipitations for a one month period (20/02-20/03) with respect to the 1990-2019 period. The standardized anomaly was computed by considering the series of accumulated precipitations for the 20/02-20/03 period for each year over 1990-2019 and removing the mean and dividing by the standard deviation. The Eastern coast of Australia saw extremely strong precipitations, with many locations exceeding 5 standard deviation anomalies with respect to the climatology.

We study whether this event can be attributed to climate change using dynamical systems theory to target the concurrent atmospheric circulation patterns and search for pattern recurrences in the far (1948-1977) and recent past (1990-2019). Our working hypothesis is that the far past acts as a counterfactual world where the Earth climate was not influenced by anthropogenic forcing when compared to the recent past (the factual world). Additionally,

we assume that the 30-year period is long enough to average out the interannual variability of the atmospheric motions (as that caused, for example, by El-Niño - Southern Oscillation). Finally we verify that these events produce similar impacts on the targeted regions.

The paper is organized as follows: section 2 describes the data and methods used in this study. This is followed by the results (Section 3) providing both a statistical a dynamical attribution analysis. We conclude with a discussion and perspectives in Section 4.

2 Data and Methods

2.1 Data

In order to detect significant changes in the circulation associated with Australian Rain bombs, we use daily sea level pressure (slp), 500hPa geopotential height ($z500$) and 2m air temperature ($t2m$) data from the NCEP/NCAR reanalysis (Kalnay et al, 1996) over the period 01/01/1948 – 31/03/2022. The data have a horizontal resolution of $2.5° \times 2.5°$.

The precipitation data are taken from the high resolution daily rainfall gridded datasets of the Bureau of Meteorology of Australia. The data have a horizontal resolution of $0.05° \times 0.05°$. Daily precipitation data from the Alderley station, close to Brisbane, is also used solely. The gridded data set will be used for the dynamical attribution (section 3.2) and the station data for the statistical attribution (section 3.1). For the ENSO index, we used the Nino3.4 detrended index as in Van Oldenborgh et al (2021).

2.2 Methods

Extreme Value Theory (EVT) has been introduced in the study of atmospheirc flows a decade ago (Freitas et al, 2008) and has gained a considerable amount of attention in both the applied mathematics and the climate science communities (Lucarini et al, 2012, 2016; Faranda et al, 2019). It can be used to compute recurrence times statistics for meteoroloical observables, but also gives access to important information on the stability and the predictability of a particular climatic state. We can apply this framework to the study how weather extremes are influenced by anthropogenic-driven climate change conditioned to the occurrence of a specific atmospheric circulation pattern (Faranda et al, 2020). Indeed weather extremes are associated with synoptic objects, i.e. a cyclone, an anticyclone, or a couple of these structures. During this identification, we select a region (a longitude/latitude box) that fits the synoptic objects that we want to examine. Once fixed the day of interest ζ, we scan all the 3-days rolling averaged sea-level pressure (slp) and 500hPa geopotential ($z500$) maps of the selected region in two periods: 1948-1977 (counterfactual world) and 1990-2019 (factual world). For both periods, we select the best 35 analogues as the slp and $z500$ maps minimizing the pointwise euclidean distance with the target day ζ. We verified that the results are not sensitive to the

choice of the number of analogues provided that we extract between 25 and 50 analog maps. 30 years long factual and counterfactual periods ensure a large enough statistical sample of slp and $z500$ maps to be able to select sufficiently authentic analogues. Furthermore, it is short enough to satisfy the assumption of climate stationarity, with respect to anthropogenic climate change, while still long enough for the interannual and interdecadal natural variability of the atmospheric circulation to be averaged over.

Once obtained the two sets of analogues for the factual and counterfactual periods, we average them out to search for significant differences Δslp and $\Delta z500$. To determine significant changes, we apply a two-tails Welch's t-test (Welch, 1947) with different variance at each grid point. We mark as significant only grid point changes for which the p-value of the test is below 0.05. Conditioning to the dates determined for slp or $z500$ maps, we also study the associated 2 meters temperatures $t2m$ and total precipitation maps tp. The Welch's t-test procedure is repeated on these ensembles to identify significant changes.

Using the dynamical systems framework described above, we then introduce a few metrics to determine the recurrence properties of the map in the counterfactual and factual worlds. These metrics are computed twice, once with the set of analogues obtained in each period. The formulas for computing these metrics are given in appendix A. For more information, please refer to Faranda et al (2022).

- Analogs Quality Q: We can study the typicality of ζ by comparing the euclidean distance of ζ from its analogues with the distances of the analogues from their own analogues. If the value of Q belongs to the same distribution of the values of Q analogues, then the typicality of the event is ensured and attribution of ζ can be performed. If instead the Q for the chosen day is larger than that of the analog days, then this is an unprecedented slp or $z500$ configuration and the results for attribution must be taken more carefully. A difference in Q between the counterfactual and factual periods indicate a change in typicality of the event due to climate change.
- Predictability Index D: Also called instantaneous dimension. For an atmospheric state ζ, $D(\zeta)$ measures the density of similar configurations. We can compute $D(\zeta)$ in both the periods to detect a climate-change induced shift in predictability. Indeed, D is a proxy for the number of degrees of freedom of the map, meaning that the higher the dimension the more unpredictable the next slp or $z500$ maps will be. If the dimension D of the chosen day is higher or lower than that of the analogues, then the day will be less or more predictable than its closest dynamical situations.
- Persistence Index Θ: Another information derived from the dynamical systems theory is the persistence of a given configuration. The persistence counts for how many days we are likely to observe a map that will resemble ζ. Once again we will compute Θ for the two different periods and using the analogs as well to detect shifts from the factual to the counterfactual worlds.

- Seasonality of Analogs: We can also simply count the number of analogs in each month to detect whether a given circulation shifts towards earlier or later months. This can have strong thermodynamic implications.

We also provide results of the attribution conditional not on the past and present climate, but on the El-Niño - Southern Oscillation (ENSO) mode. ENSO is known to be a major factor in the variability of tropical and sub-tropical regions around the Pacific and likely played a role in the February 2022 event for which the mode was strongly negative. Therefore, we decided to run the attribution analysis conditional on the Nino3.4 index being above the 75% percentile (ENSO+) and below the 25% percentile (ENSO-) for the period 1948-2019. Analogues are then computed in those two pools of data using either 3-days rolling averaged *slp* or $z500$ maps.

3 Results

3.1 Statistical attribution

In order to assess the possible changes in the probability of occurrence for the event due to climate change, we use the rapid statistical attribution method described in Section 2. We fit the 3-days averaged precipitation yearly maxima to a Generalized Extreme Value (GEV) law for the factual and counterfactual periods for three stations, namely the Alderley station (Brisbane) at the epicentre of the 26th-28th February event, the Sydney Botanic garden station and the Cairns Aero station . We repeat the same analysis over the region 152°-154°W, 25.5°-31°S centered on Brisbane where the event was the most extreme (see, e.g. Figure 1b) .

Figure 2 shows the resulting GEV fits for Brisbane (a), Brisbane region (b), Sydney (c) and Cairns (d). In both the factual and counterfactual worlds the event of April 2022 in Brisbane was exceptional, with return periods estimated of more than a thousand years. The event was also a 100-year precipitation event in the Brisbane region in both periods. The 26th-28th February event was less extreme in Sydney and Cairns, with return periods of less than a decade in both stations for the factual and counterfactual periods. In Alderley station return levels are slightly higher in the counterfactual period. We can explain this by the occurrence of an extreme precipitation events in January 1974, that also produced floods in Brisbane. However, the 95% confidence intervals are too wide to conclude to any detectable effect of climate change with this method.

Figure 3 shows the same analysis but conditioned to the phases of El Niño Southern oscillation. In particular, we condition using Nino 3.4 index, sampling ENSO+ phases and ENSO- phase, defined respectively as the first and last quartile of the index. Results show a stronger effect of the la Niña phase (ENSO-) on precipitation rates at both Brisbane stations (3a). The 2022 26th to 28th February event is very rare during ENSO+ phases with a return period of over 400 years. Instead, it has a return period of 120 years in ENSO- phases.

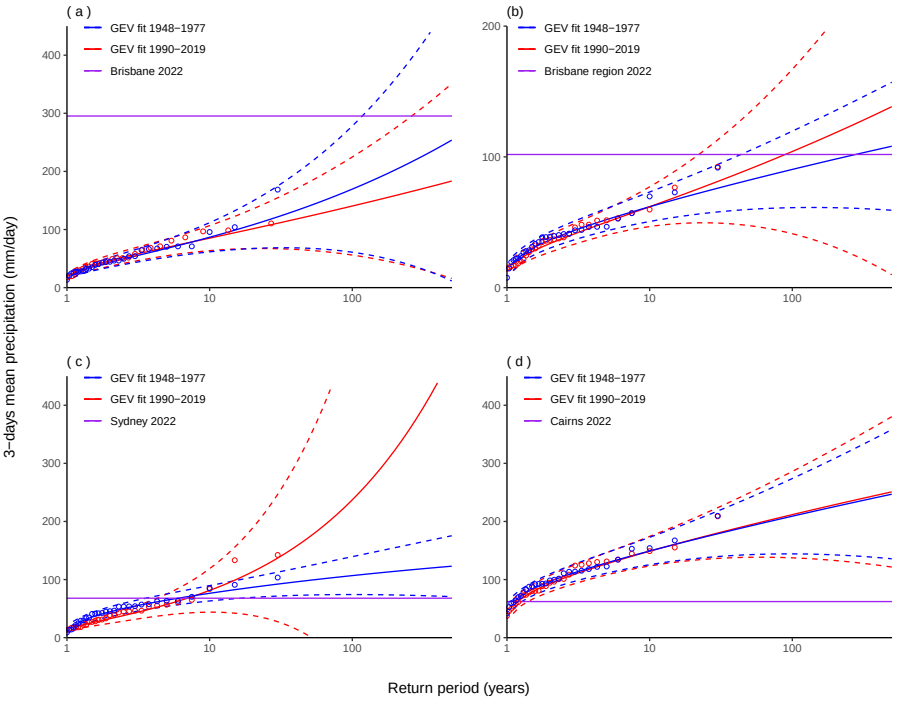

Fig. 2 Fit of the annual maximum of 3-days averaged precipitation running means at Brisbane (Alderley station) (a), the Brisbane region (152°-154°W, 25.5°-31°S) (b), Sydney (Sydney Botanic gardens station) (c) and Cairns (Cairns Aero station) (d) to a GEV in the factual and counterfactual periods. Gumbel plot of the GEV fit over 1948-1977 (blue lines with 95% confidence intervals), and 1992-2021 (red lines) using the maximum likelihood estimation. The purple line shows the value of intensity of the observed event at the station or area of interest in 2022.

This is in agreement with the influence of the strong la Niña phase currently ongoing on the intensity of the 2022 event suggested in 1. This effect is less clear if we consider the Brisbane region (3b): in this case the confidence intervals are so wide that it is difficult to draw any conclusion. The same procedure applied to Sydney (3c) and Cairns (3d) station data does not allow to draw any conclusion because of the wide confidence intervals, wich prevent to obtain statistical significant differences, at least at the 95% level chosen in this study.

3.2 Dynamical attribution

To identify the dynamical and thermodynamic factors which may have played a role in the intensity of the event, we ran the dynamical attribution framework presented previously.

Figures 4 and 5 present the results using respectively *slp* and $z500$ analogues. These figures display the $slp/z500$ (a–d), $t2m$ (e–h) and *prate* (i–l) maps and, from left to right, the maps of the event (a,e,i), the composites of

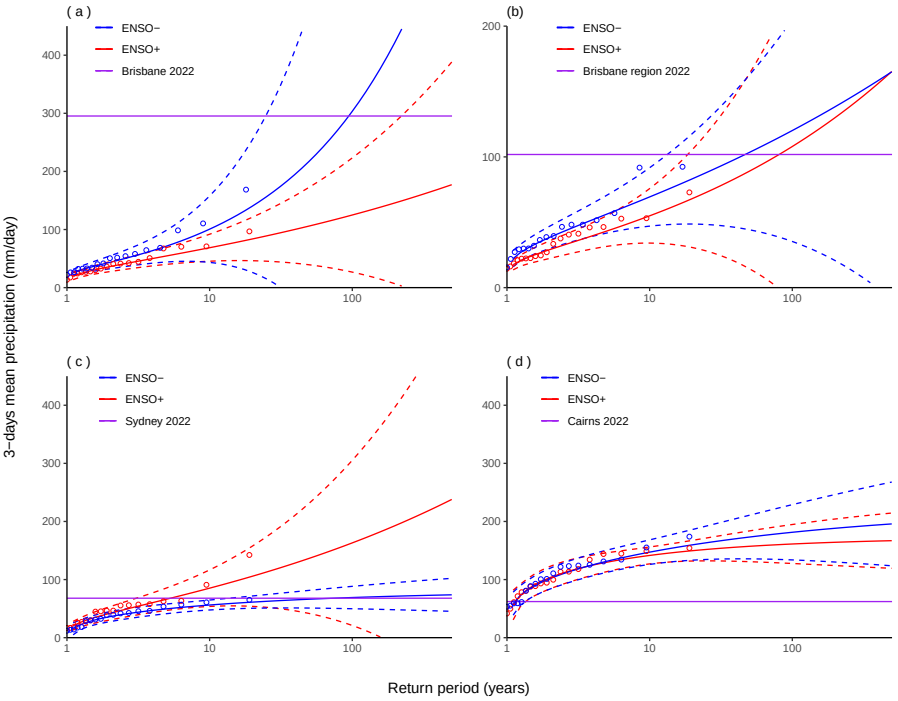

Fig. 3 Fit of the annual maximum of 3-days averaged precipitation running means at Alderley station (a) and over the Brisbane region (152°-154°W, 25.5°-31°S) (b) to a GEV, depending on El Niño 3.4 detrended index. Gumbel plot of the GEV fit over years in the 1st quartile (red lines) and 4th quartile (blue lines) of NINO3.4 index average over JFM from 1948 to 2021, with 95% confidence intervals. The purple line shows the value of intensity of the observed event at Alderley station in 2022.

counterfactual (b,f,j) and factual (c,g,k) analogs and the difference between the factual and counterfactual analogs (d,h,l) where hashed-filled areas show significant differences. Distributions of additional metrics comparing the counterfactual and factual periods, namely analogs quality, predictability, persistence and distribution by season are shown in panels m–p, respectively.

For the *slp* analogues, we firstly notice that the analogues quality (Q) is not good and therefore results must be interpreted carefully (panel (m)). In the factual period, there is a signal of intensified high-pressures over New Zealand, which may be related to the stronger advection of moist air from the Coral sea. When we look at the precipitation difference map (Fig. 4 (l)), there are indeed stronger precipitations on the Eastern coast of Australia in the factual period but only few regions are significantly different than the counterfactual period and do not fully correspond to the regions where the precipitations are maximum during the February 2022 event. There is moreover no strong temperature signal as depicted in panel (h) using 2m air temperature which does not display significant differences between the factual and counterfactual periods on the Eastern coast and in the Coral sea. However, panel (o) and (p)

show that the predictably is lower and the persistence is higher in the factual period. The event is particularly persistent compared to its analogues in the factual period which may explain the intensity of the event.

This results are confirmed when using the $z500$ analogues (Fig. 5), which are better as shown in panel (m). The factual period displays stronger high $z500$ over the northern region but also almost no significant temperature signal (panel (h)). The low predictability D (panel (n)) but high persistence Θ (panel (p)) of the event is also noticed using $z500$ analogues. When it comes to precipitations, even though they are stronger during the factual period (panel (l)), this difference is not significant.

These results are coherent with the statistical attribution in so far as the temperature signal associated with climate change is weak. There is however a noticeable dynamical signal in the two periods as represented in the *slp* and $z500$ analogues difference maps. One may indeed notice that ENSO, which is the major driver of variability in the region, was in a strong and persistent La Nina phase during the event, which is not fully represented using analogues (see figure 6). We therefore decided to run the same dynamical attribution analysis using the Nino3.4 index to define ENSO- phases and factual ENSO+ phases.

The results of this analysis are presented in figures 7 and 8 using respectively *slp* and $z500$ analogues. On the dynamical side, there is a significant stronger upper level low during ENSO- phases (Fig. 8 panel (d)) analogues. Using both analogues, the temperature signal is much stronger during ENSO+ phases, which may explain the absence of signal when doing the analysis during past and present periods: the natural variability is stronger than the climate change signal on this region. When it comes to precipitations, there is a strong positive signal on the Eastern coast and Brisbane regions during La Nina phases using *slp* analogues but the quality of analogues is low and these results are not significant using $z500$ analogues.

4 Conclusions

In this paper we have performed a statistical and dynamical attribution of the Australian rain bomb event of February 2022. We have used both reanalyses and historical records of daily precipitations in the past (1948-1977, counterfactual) and present (1990-2019, factual) periods. From a statistical point of view, this extreme precipitation event was unprecedented in the Brisbane region and very intense with respects to previous historical records in the broader Eastern coast of Australia. The statistical attribution suggests that this event has a low probability to happen both in the past and present climate (less than one in a century). There is no clear signal of a climate change influence (high uncertainty) which translates in a low evidence for the attribution of this event to climate change.

The dynamical attribution, performed using the method of analogues circulation patterns proposed in Faranda et al (2022) to those observed during the

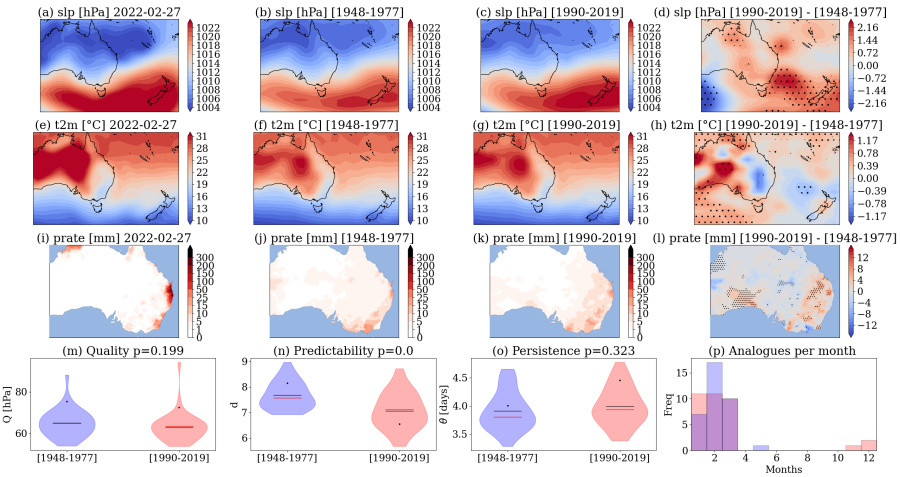

Fig. 4 Dynamical attribution using *slp* analogues for the Australian rain bomb on 27-02-2022. 3-days rolling mean sea-level pressure *slp* (a), 2-meter temperatures $t2m$ (e) and total precipitation *prate* (i) centered on the 27-02-2022. Average of the 35 sea-level pressure analogs found for the counterfactual [1948-1977] (b) and factual [1990-2019] (c) periods and corresponding 2-meter temperatures (f,g) and daily precipitation rate (j,k). Δslp (d), $\Delta t2m$ (h) and $\Delta prate$ (i) between factual and counterfactual periods: hashed-filled areas show significant differences. Violin plots for counterfactual (blue) and factual (red) periods for the Analogs Quality Q (m) the Predictability index D (n), the Persistence index θ (o) and the distribution of analogs in each month (p). Values for the selected day are marked by a black dot. Black (resp. red) lines represent the empirical mean (resp. median) of the distribution.

events suggest the exceptional characteristics of the event which appears to be unprecedented in both the factual and counterfactual distributions of weather patterns: it has arisen as the combination of ingredients: the tropical moisture was deflected to the subtropics, collected and lifted by a low pressure system which stationed over Eastern Australia blocked by an high pressure offshore the Coral sea. This combination created an atmospheric river capable of transporting several gigaliters of water towards the Queensland and the South West of the continent. Finally, La Niña phase of the El-Niño-Southern-Oscillation likely played a significant role in the intensity of the event.

The main limitation of this study is that we do not use climate models: the rational for doing so comes from the evidence that both large, regional and local phenomena contributed to this event. In order to perform an attribution study based on models, we would need a large ensemble of convection permitting models resolving at least the region shown in Fig. 1, with specific runs capable to evaluate also the contribution of la Nina to the event. Even with such models, the detailed physics of the precipitation could still depend on the microphysics introduced in the model as shown by Ban et al (2021). A further limitation of this study is the use of factual and counterfactual periods consisting of only 30 years. While we could in principle consider the whole period twice, as in the protocol described by Philip et al (2020), we cannot

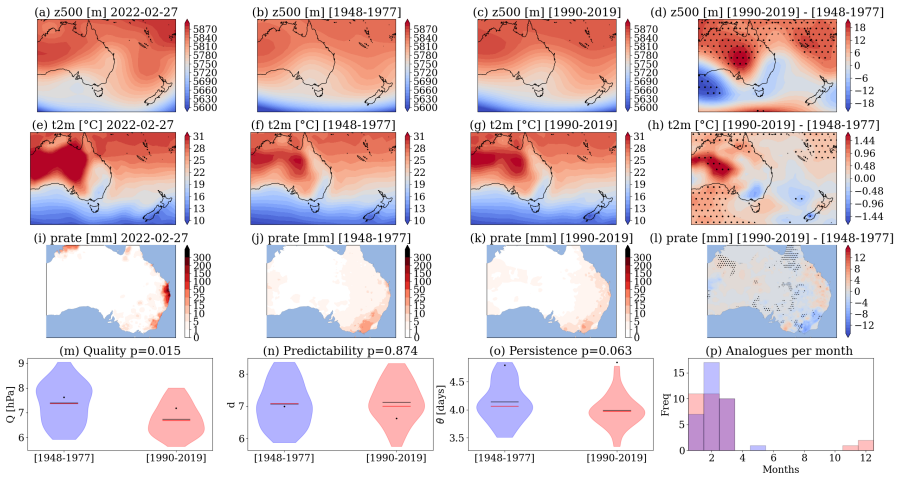

Fig. 5 Dynamical attribution using $z500$ analogues for the Australian rain bomb on 27-02-2022. 3-days rolling mean 500hPa geopotential height $z500$ (a), 2-meter temperatures $t2m$ (e) and total precipitation $prate$ (i) centered on the 27-02-2022. Average of the 35 500hPa geopotential height analogs found for the counterfactual [1948-1977] (b) and factual [1990-2019] (c) periods and corresponding 2-meter temperatures (f,g) and daily precipitation rate (j,k). $\Delta z500$ (d), $\Delta t2m$ (h) and $\Delta prate$ (i) between factual and counterfactual periods: hashed-filled areas show significant differences. Violin plots for counterfactual (blue) and factual (red) periods for the Analogs Quality Q (m) the Predictability index D (n), the Persistence index θ (o) and the distribution of analogs in each month (p). Values for the selected day are marked by a black dot. Black (resp. red) lines represent the empirical mean (resp. median) of the distribution.

here use the implicit assumption of stationarity of the variability of the rainfall extremes that is underlying the protocol. While this is a limitation on the available data, it is a fair way to account for the variability of extremes, allowing for a larger uncertainty and a conservative estimates on the role of climate change to triggering this event.

To frame our results in a more general framework, we observe that they are in line with what the IPCC report AR6, WG1, Chapter 11.4, states about rainfall over the region, namely that "Available evidence has not shown an increase or a decrease in heavy precipitation over Australasia as a whole (medium confidence), but heavy precipitation tends to increase over Northern Australia (particularly the north-west) and decrease over the eastern and southern regions." (Seneviratne et al, 2021) . We however observe that the compounding dynamical elements driving this event are also observed in a series of unprecedented extreme weather events occurred in the last few years, including the 2021 Canada heat dome, the Antarctica atmospheric rivers, the 2022 Indian, Chines, Western European and North American heatwaves. Such series of record breaking events raise the question of the emergence of new phenomena linked to global warming, a field to explore statistically, e.g. by using the concept of time of emergence introduced in Hawkins and Sutton (2012)

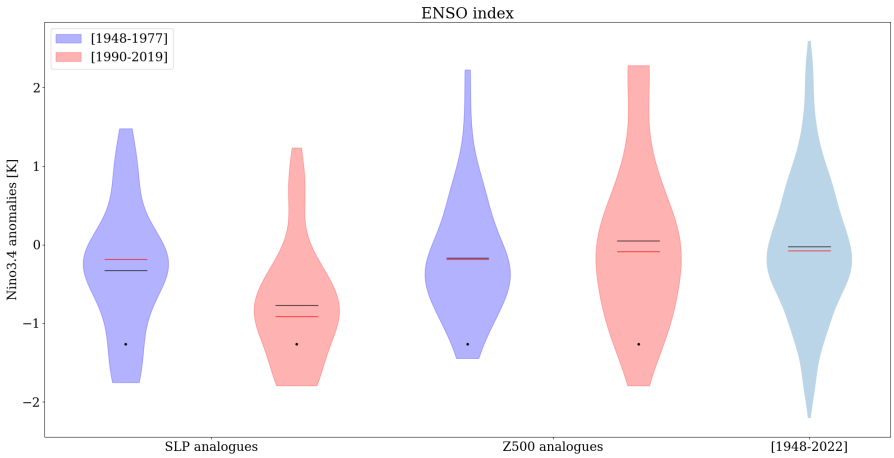

Fig. 6 Distribution of ENSO index between factual and counterfactual periods for the two types of analogues. Blue (resp. red) violin plots represent the distribution of the ENSO index for the analogues in the counterfactual (resp. factual) period. The red (resp. black) line depicts the median (resp. mean) of the distribution. The black dot corresponds to the value of the ENSO index during the February 2022 event. The last violin plot depicts the distribution of the ENSO index for all dates between 1948 and 2019.

and dynamically, e.g. by looking the possible presence of tipping elements in the climate system (Lenton et al, 2008).

Acknowledgments. We acknowledge the Bureau of Meteorology of Australia for their help in obtaining the high resolution daily rainfall gridded datasets. The authors acknowledge the support of the INSU-CNRS-LEFE-MANU grant (project DINCLIC), as well as the gran ANR-19-ERC7-0003 (BOREAS). This work has received support from the European Union's Horizon 2020 research and innovation programme under grant agreement No. 101003469 (XAIDA) and the Marie Sklodowska-Curie grant agreement No. 956396 (EDIPI).

Declarations

- Funding: This project has received funding from the European Union's Horizon 2020 research and innovation programme under the Marie Sklodowska-Curie grant agreement N° 956396 under grant agreement No. 101003469 (XAIDA).
- Conflict of interest: The authors declare no conflict of interest.
- Ethics approval: Not applicable.
- Consent to participate: Not applicable.
- Consent for publication: Not applicable.
- Availability of data and materials: NCEP data are available on the NOAA website at https://psl.noaa.gov/data/gridded/data.ncep.reanalysis.

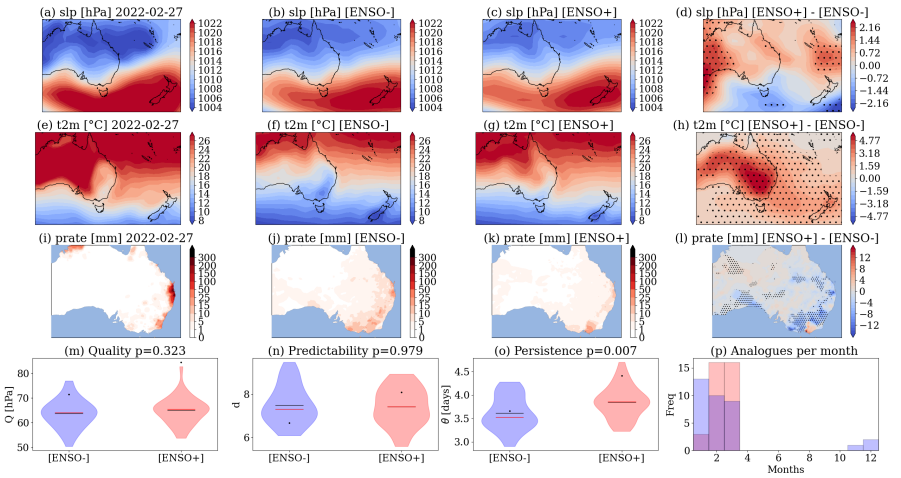

Fig. 7 Dynamical attribution using *slp* analogues for the Australian rain bomb on 27-02-2022 relative to the ENSO index. 3-days rolling mean 500hPa geopotential height $z500$ (a), 2-meter temperatures $t2m$ (e) and total precipitation *prate* (i) centered on the 27-02-2022. Average of the 35 sea-level pressure analogs found for the counterfactual [ENSO-] (b) and factual [ENSO+] (c) periods and corresponding 2-meter temperatures (f,g) and daily precipitation rate (j,k). $\Delta z500$ (d), $\Delta t2m$ (h) and $\Delta prate$ (i) between factual and counterfactual periods: hashed-filled areas show significant differences. Violin plots for counterfactual (blue) and factual (red) periods for the Analogs Quality Q (m) the Predictability index D (n), the Persistence index θ (o) and the distribution of analogs in each month (p). Values for the selected day are marked by a black dot. Black (resp. red) lines represent the empirical mean (resp. median) of the distribution.

html. Rainfall data over Australia are available at the National Computational Infrastructure (NCI) THREDDS server at https://dapds00.nci.org.au/thredds/catalog/zv2/agcd/v1/precip/total/r005/01day/catalog.html.

- Code availability: The main results of this work were obtained using Python. The scripts are available upon request.
- Authors' contributions: CC, NM and RN performed the analysis. DF designed the analyses. All authors participated to the manuscript preparation and writing.

A Predictability and Persistence Indices

The attractor of a dynamical system is a geometric object defined in the space hosting all the possible states of the system (phase-space). Each point ζ on the attractor can be characterized by two dynamical indicators: the local dimension D, which indicates the number of degrees of freedom active locally around ζ, and the persistence Θ, a measure of the mean residence time of the system around ζ (Faranda et al, 2017). To determine D, we exploit recent results from the application of extreme value theory to Poincaré recurrences in dynamical systems. This approach considers long trajectories of a system — in our

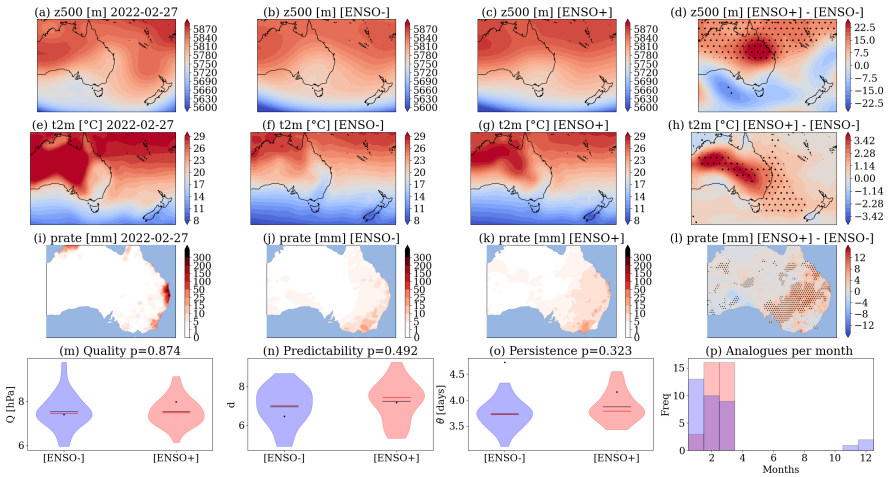

Fig. 8 Dynamical attribution using $z500$ analogues for the Australian rain bomb on 27-02-2022 relative to the ENSO index. 3-days rolling mean 500hPa geopotential height $z500$ (a), 2-meter temperatures $t2m$ (e) and total precipitation $prate$ (i) centered on the 27-02-2022. Average of the 35 500hPa geopotential-https://www.overleaf.com/project/627ba03eceee706667e9e0ca height analogs found for the counterfactual [ENSO-] (b) and factual [ENSO+] (c) periods and corresponding 2-meter temperatures (f,g) and daily precipitation rate (j,k). $\Delta z500$ (d), $\Delta t2m$ (h) and $\Delta prate$ (i) between factual and counterfactual periods: hashed-filled areas show significant differences. Violin plots for counterfactual (blue) and factual (red) periods for the Analogs Quality Q (m) the Predictability index D (n), the Persistence index θ (o) and the distribution of analogs in each month (p). Values for the selected day are marked by a black dot. Black (resp. red) lines represent the empirical mean (resp. median) of the distribution.

case successions of daily SLP latitude–longitude maps — corresponding to a sequence of states on the attractor. For a given point ζ in phase space (e.g., a given SLP map), we compute the probability that the system returns within a ball of radius ϵ centered on the point ζ. The Freitas et al (2010) theorem, modified by Lucarini et al (2012), states that logarithmic returns:

$$g(x(t)) = -\log(\mathrm{dist}(x(t), \zeta)) \tag{1}$$

yield a probability distribution such that:

$$\Pr(z > s(q)) \simeq \exp\left[-\vartheta(\zeta)\left(\frac{z-\mu(\zeta)}{\sigma(\zeta)}\right)\right] \tag{2}$$

where $z = g(x(t))$ and s is a high threshold associated to a quantile q of the series $g(x(t))$. Requiring that the orbit falls within a ball of radius ϵ around the point ζ is equivalent to asking that the series $g(x(t))$ is over the threshold s; therefore, the ball radius ϵ is simply $e^{-s(q)}$. The resulting distribution is the exponential member of the Generalized Pareto Distribution family. The parameters μ and σ, namely the location and the scale parameter of the distribution, depend on the point ζ in phase space. $\mu(\zeta)$ corresponds to the threshold $s(q)$ while the local dimension $D(\zeta)$ can be obtained via the

relation $\sigma = 1/D(\zeta)$. This is the metric of predictability introduced in Sect. 2.2.

When $x(t)$ contains all the variables of the system, the estimation of D based on extreme value theory has a number of advantages over traditional methods (e.g. the box counting algorithm (Liebovitch and Toth, 1989; Sarkar and Chaudhuri, 1994)). First, it does not require to estimate the volume of different sets in scale-space: the selection of $s(q)$ based on the quantile provides a selection of different scales s which depends on the recurrence rate around the point ζ. Moreover, it does not require the a priori selection of the maximum embedding dimension as the observable g is always a univariate time-series.

The persistence of the state ζ is measured via the extremal index $0 < \vartheta(\zeta) < 1$, an adimensional parameter, from which we extract $\Theta(\zeta) = \Delta t/\vartheta(\zeta)$. Here, Δt is the timestep of the dataset being analysed. $\Theta(\zeta)$ is therefore the average residence time of trajectories around ζ, namely the metric of persistence introduced in Sect. 2.2, and it has unit of a time (in this study days). If ζ is a fixed point of the attractor, then $\Theta(\zeta) = \infty$. For a trajectory that leaves the neighborhood of ζ at the next time iteration, $\Theta = 1$. To estimate ϑ, we adopt the Süveges estimator (Süveges, 2007). For further details on the the extremal index, see Moloney et al (2019).

References

Abram NJ, Henley BJ, Sen Gupta A, et al (2021) Connections of climate change and variability to large and extreme forest fires in southeast australia. Communications Earth & Environment 2(1):1–17

Ban N, Caillaud C, Coppola E, et al (2021) The first multi-model ensemble of regional climate simulations at kilometer-scale resolution, part i: evaluation of precipitation. Climate Dynamics 57(1):275–302

Borchers Arriagada N, Palmer AJ, Bowman DM, et al (2020) Unprecedented smoke-related health burden associated with the 2019–20 bushfires in eastern australia. Medical Journal of Australia 213(6):282–283

Canadell JG, Meyer C, Cook GD, et al (2021) Multi-decadal increase of forest burned area in australia is linked to climate change. Nature communications 12(1):1–11

Church JA, Hunter JR, McInnes KL, et al (2006) Sea-level rise around the australian coastline and the changing frequency of extreme sea-level events. Australian Meteorological Magazine 55(4):253–260

Church JA, McInnes KL, Monselesan D, et al (2017) Sea level rise and allowances for coastal councils around australia–guidance material

ClimateCouncilAustralia (2022) A supercharged climate: Rain bombs, flash flooding and destruction. Available at https://www.climatecouncil.org.au/resources/supercharged-climate-rain-bombs-flash-flooding-destructionAccessed: 08/07/2022

Cook BI, Mankin JS, Anchukaitis KJ (2018) Climate change and drought: From past to future. Current Climate Change Reports 4(2):164–179

Dey R, Lewis SC, Arblaster JM, et al (2019) A review of past and projected changes in australia's rainfall. Wiley Interdisciplinary Reviews: Climate Change 10(3):e577

Douville H, Raghavan K, Renwick J, et al (2021) Water Cycle Changes. In Climate Change 2021: The physical science basis. contribution of Working Group I to the Sixth Assessment Report of the Intergovernmental Panel on Climate Change

Faranda D, Messori G, Yiou P (2017) Dynamical proxies of north atlantic predictability and extremes. Scientific reports 7:41,278

Faranda D, Alvarez-Castro MC, Messori G, et al (2019) The hammam effect or how a warm ocean enhances large scale atmospheric predictability. Nature communications 10(1):1–7

Faranda D, Vrac M, Yiou P, et al (2020) Changes in future synoptic circulation patterns: consequences for extreme event attribution. Geophysical Research Letters 47(15):e2020GL088,002

Faranda D, Bourdin S, Ginesta M, et al (2022) A climate-change attribution retrospective of some impactful weather extremes of 2021. Weather and Climate Dynamics Discussions pp 1–37

Filkov AI, Ngo T, Matthews S, et al (2020) Impact of australia's catastrophic 2019/20 bushfire season on communities and environment. retrospective analysis and current trends. Journal of Safety Science and Resilience 1(1):44–56

Foreign Policy (2022) The 'rain bomb' that could shape the australian election. Available at https://foreignpolicy.com/2022/03/11/australia-flood-election-climate-change/ Accessed: 08/07/2022

Freitas ACM, Freitas JM, Todd M (2008) Hitting time statistics and extreme value theory. 0804.2887

Freitas ACM, Freitas JM, Todd M (2010) Hitting time statistics and extreme value theory. Probability Theory and Related Fields 147(3-4):675–710

514 Grainger S, Fawcett R, Trewin B, et al (2022) Estimating the uncertainty
515 of australian area-average temperature anomalies. International Journal of
516 Climatology 42(5):2815–2834

517 Hawkins E, Sutton R (2012) Time of emergence of climate signals. Geophysical
518 Research Letters 39(1)

519 Head L, Adams M, McGregor HV, et al (2014) Climate change and australia.
520 Wiley Interdisciplinary Reviews: Climate Change 5(2):175–197

521 Hirabayashi Y, Mahendran R, Koirala S, et al (2013) Global flood risk under
522 climate change. Nature climate change 3(9):816–821

523 Hobday AJ, Pecl GT, Fulton B, et al (2018) Climate change impacts,
524 vulnerabilities and adaptations: Australian marine fisheries

525 Holland MM, Smith JA, Everett JD, et al (2020) Latitudinal patterns in
526 trophic structure of temperate reef-associated fishes and predicted conse-
527 quences of climate change. Fish and Fisheries 21(6):1092–1108

528 Jetten J, Fielding KS, Crimston CR, et al (2021) Responding to climate
529 change disaster: The case of the 2019/2020 bushfires in australia. European
530 Psychologist 26(3):161

531 Kalnay E, Kanamitsu M, Kistler R, et al (1996) The ncep/ncar 40-year reanal-
532 ysis project. Bulletin of the American meteorological Society 77(3):437–472

533 Lenton TM, Held H, Kriegler E, et al (2008) Tipping elements in the
534 earth's climate system. Proceedings of the national Academy of Sciences
535 105(6):1786–1793

536 Liebovitch LS, Toth T (1989) A fast algorithm to determine fractal dimen-
537 sions by box counting. physics Letters A 141(8-9):386–390. ISBN: 0375-9601
538 Publisher: Elsevier

539 Lucarini V, Faranda D, Wouters J (2012) Universal behaviour of extreme value
540 statistics for selected observables of dynamical systems

541 Lucarini V, Faranda D, Freitas ACM, et al (2016) Extremes and recurrence in
542 dynamical systems. 1605.07006

543 Masson-Delmotte V, Zhai P, Pirani A, et al (2021) Ipcc The physical science
544 basis. contribution of working group I to the Sixth Assessment Report of
545 the Intergovernmental Panel on Climate Change

546 Moloney NR, Faranda D, Sato Y (2019) An overview of the extremal index.
547 Chaos: An Interdisciplinary Journal of Nonlinear Science 29(2):022,101

Philip S, Kew S, van Oldenborgh GJ, et al (2020) A protocol for probabilistic extreme event attribution analyses. Advances in Statistical Climatology, Meteorology and Oceanography 6(2):177–203

Sarkar N, Chaudhuri BB (1994) An efficient differential box-counting approach to compute fractal dimension of image. IEEE Transactions on systems, man, and cybernetics 24(1):115–120

Seneviratne S, Zhang X, Adnan M, et al (2021) Weather and climate extreme events in a changing climate. In Climate Change 2021: The physical science basis. contribution of Working Group I to the Sixth Assessment Report of the Intergovernmental Panel on Climate Change

Süveges M (2007) Likelihood estimation of the extremal index. Extremes 10(1-2):41–55

The Guardian (2022) 'this is an emergency': Australia's extreme weather crises spark anger at climate inaction. Available at https://www.theguardian.com/australia-news/2022/apr/09/this-is-an-emergency-australias-extreme-weather-crises-spark-anger-at-climate-inaction Accessed: 08/07/2022

The New Daily (2022) 'very unusual': Australia's east coast cities are feeling their coldest start to winter in decades. Available at https://thenewdaily.com.au/news/national/2022/06/09/cold-winter-weather-australia Accessed: 08/07/2022

Ukkola AM, De Kauwe MG, Roderick ML, et al (2020) Robust future changes in meteorological drought in cmip6 projections despite uncertainty in precipitation. Geophysical Research Letters 47(11):e2020GL087,820

Van Oldenborgh GJ, Hendon H, Stockdale T, et al (2021) Defining el niño indices in a warming climate. Environmental research letters 16(4):044,003

Welch BL (1947) The generalization of 'student's'problem when several different population varlances are involved. Biometrika 34(1-2):28–35

Wilby RL, Keenan R (2012) Adapting to flood risk under climate change. Progress in physical geography 36(3):348–378

Wolff NH, Mumby PJ, Devlin M, et al (2018) Vulnerability of the great barrier reef to climate change and local pressures. Global change biology 24(5):1978–1991

Woodruff JD, Irish JL, Camargo SJ (2013) Coastal flooding by tropical cyclones and sea-level rise. Nature 504(7478):44–52